Computers in Biology and Medicine 109 (2019) 70–78

Contents lists available at ScienceDirect

Computers in Biology and Medicine

journal homepage: www.elsevier.com/locate/compbiomed

On the role of material properties in ascending thoracic aortic aneurysms

Federica Cosentino[a,b], Valentina Agnese[c], Giuseppe M. Raffa[c], Giovanni Gentile[c], Diego Bellavia[c], Massimiliano Zingales[d], Michele Pilato[c], Salvatore Pasta[b,c,*]

[a] Biomedical Department of Internal Medicine and Specialities (DIBIMIS), Piazza delle Cliniche, n.2, 90128, University of Palermo, Palermo, Italy
[b] Fondazione Ri.MED, Via Bandiera n.11, 90133, Palermo, Italy
[c] Department for the Treatment and Study of Cardiothoracic Diseases and Cardiothoracic Transplantation, IRCCS-ISMETT, Via Tricomi n.5, 90127, Palermo, Italy
[d] Department of Civil, Environmental, Aerospace, Materials Engineering (DICAM), Viale delle Scienze Ed.8, 90128, University of Palermo, Palermo, Italy

ARTICLE INFO

Keywords:
Ascending aortic aneurysm
Inverse approach
Material parameters
Aortic aneurysm failure
Finite-element analysis

ABSTRACT

One of the obstacles standing before the biomechanical analysis of an ascending thoracic aortic aneurysm (ATAA) is the difficulty in obtaining patient-specific material properties. This study aimed to evaluate differences on ATAA-related stress predictions resulting from the elastostatic analysis based on the optimization of arbitrary material properties versus the application of patient-specific material properties determined from *ex-vivo* biaxial testing. Specifically, the elastostatic analysis relies the on the fact that, if the aortic wall stress does not depend on material properties, the aorta has to be statistically determinate. Finite element analysis (FEA) was applied to a group of nine patients who underwent both angio-CT imaging to reconstruct ATAA anatomies and surgical repair of diseased aorta to collect tissue samples for experimental material testing. Tissue samples cut from excised ATAA rings were tested under equibiaxial loading conditions to obtain experimentally-derived material parameters by fitting stress-strain profiles. FEAs were carried out using both optimized and experimentally-derived material parameters to predict and compare the stress distribution using the mean absolute percentage error (MAPE). Although physiological strains were below yield point (range of 0.08–0.25), elastostatic analysis led to errors on the stress predictions that depended on the type of constitutive model (highest MAPE of 0.7545 for Yeoh model and 0.7683 for Fung model) and ATAA geometry (lowest MAPE of 0.0349 for patient P.7). Elastostatic analysis needs better understanding of its application for determining aneurysm mechanics, and patient-specific material parameters are essential for reliable accurate stress predictions in ATAAs.

1. Introduction

A ruptured ascending thoracic aortic aneurysm (ATAA) is considered a surgical emergency since progressive dilatation is often fatal if this disease is not detected by diagnostic imaging and managed immediately [1]. Despite being a relatively rare event with an estimated incidence of 5.0 per 100,000 individuals per year, the risk of fatal complications such as rupture or acute dissections can be as high as 50% in patients with a large ATAA wall (aortic diameter > 50 mm) [2,3]. The risk over time of ATAA development to a size of 40–45 mm in patients with a congenital bicuspid aortic valve (BAV) versus the morphological normal tricuspid aortic valve (TAV) is remarkable. Several studies highlighted that 84% of individuals with BAV may develop aortopathy during the life course [4,5]. With regards to ATAA, degenerative aneurysms tend to develop in the mid-ascending aorta and then progress distally and proximally while ATAAs associated with connective tissue disorders are usually confined to the aortic root [6].

Although the aortic size criterion can be adjusted to achieve higher patient specificity using the body surface area or patient height [7], the surgical dilemma still exists because fatal complications can occur at aortic diameters lower than that dictated by current clinical guidelines for elective repair of aneurysmal aorta [8]. There is a need to delineate additional metrics, not based on aortic size, to better identify the risk of ATAA failure. Biomechanical risk assessments using finite element analysis (FEA) to estimate the wall stress exerted on the diseased aorta have been proposed in abdominal aortic aneurysms [9,10] and ATAAs [11,12]. These approaches for risk stratification appeared to be promising since peak wall stress can be calculated from routinely performed CT scans and may be a better predictor of risk of rupture than aortic diameter [13]. Recently, FEA was combined with machine learning techniques to study the relationship between shape features and wall stress as risk metric of ATAA, towards the development of computer-aided-diagnosis [14].

FEAs depend on several factors including the aortic geometry, the

* Corresponding author. Professor of Industrial Bioengineering, Fondazione Ri.MED, Italy.
E-mail address: spasta@fondazionerimed.com (S. Pasta).

https://doi.org/10.1016/j.compbiomed.2019.04.022
Received 1 March 2019; Received in revised form 20 April 2019; Accepted 20 April 2019
0010-4825/

loading condition induced by hemodynamic and structural loads and the material properties of aortic wall constituents. Hemodynamic can be evaluated by computational fluid dynamic [15–18] or *in-vivo* 4D flow MRI [19] while tracking algorithms of aortic wall surface detected by dynamic CT [20] or MRI [21] can be adopted to estimate the ATAA-related structural mechanics. Obtaining material parameters non-invasively during patient monitoring for preoperative risk estimations represent an important challenge. However, if the stress distribution does not depend on material properties, the structure has to be statically determinate [22,28]. Under this condition, we can eliminate the need for patient-specific material properties and the FEA can be performed with arbitrary material properties because they do not affect the resulting wall stress. Several research groups adopted this approach to compute wall stress of abdominal [22] and ascending aortic aneurysms [23–26].

In this proof-of-concept, we want to know how different would be the resulting stress distribution on the aneurysm wall if material properties derived by an elastostatic analysis proposed by Liu et al. [23] are used as compared to FEAs using patient-specific material properties determined from *ex-vivo* biaxial testing. If large differences of stress distributions are observed, one could raise a red flag for further investigation using this appealing approach. To accomplish this task, we carried out FEAs on nine patients who underwent both dynamic CT imaging and surgical elective repair of ATAA to both reconstruct aortic geometries for FEA and collect tissue samples for patient-specific material property evaluation by the fitting of experimental stress-strain curves. Both an isotropic- (ie, two-term Yeoh model) and an anisotropic (ie, Fung-exponential model) constitutive formulation were tested. A stress comparison using the optimal material set versus the experimentally-derived material set was performed, and results were discussed.

2. Methods

2.1. Study population

All nine patients included in this investigation had electrocardiogram-gated computed tomography angiography (ECG-gated CT) for the measurement of the maximum aortic diameter and then elective surgical repair of dilated aortas at ISMETT IRCCS hospital institution. ECG-gated CT scans were reconstructed to obtain images at both diastolic and systolic cardiac phases, which were used for the estimation of the diastolic-to-systolic displacement field of the aortic wall. This displacement field was used as a boundary condition for FEA as previously described by our group [27]. Aortic valve shape was classified as TAV versus BAV based on reconstructed images parallel to the aortic valve plane. The presence of the raphe was used to group BAV morphology according to the fusion of right and left cusps (AP) as well as the fusion of right and non-coronary cusp (RL). After surgical ATAA repair, excised aortic tissues were stored in a physiologic solution upon biaxial mechanical testing. Table 1 shows patient demographic information, pre-operative aortic diameters and thickness measurements. The study was approved by the local research ethics committee, and all patients signed informed consent prior enrollment.

Table 1
Patient demographic information.

Patient ID	Age	Gender	Aortic Valve	Type	Systolic Diameter (mm)	Diastolic Diameter (mm)	Thickness (mm)
P.1	70	Male	BAV	AP	52.0	51.2	2.1
P.2	71	Male	TAV	/	50.4	50.8	1.9
P.3	67	Male	TAV	/	54.8	57.1	2.2
P.4	56	Male	BAV	RL	52.4	53.6	1.8
P.5	58	Male	TAV	/	42.3	45.2	2.2
P.6	67	Male	TAV	/	48.5	49.8	2.8
P.7	78	Male	TAV	/	46.5	47.8	2.1
P.8	63	Female	TAV	/	54.8	55.8	1.7
P.9	68	Male	TAV	/	44.7	45.1	2.3

2.2. Biaxial testing

Experimentally-related material properties from aneurysmal tissue samples collected for each patient were estimated by equibiaxial mechanical testing using an ElectroForce TestBench system (TA Instrument, Boston, MA). In brief, square specimens (10 × 10mm) cut form the tissue region located along the major curvature of the aortic ring were extrapolated. Each specimen was oriented along longitudinal and circumferential directions of the aortic vessel while sutures were used to fix specimen edge using surgical staples. Thickness was measured with a caliper for each sample (see Table 1). Five black markers were placed on the intimal aortic tissue surface to evaluate engineering strains along testing directions using a digital video extensometer placed perpendicular to the testing area. During biaxial loading, the specimen was sub-merged in 0.9% physiologic saline solution in a bath under controlled temperature of 37 °C. A small preload (0.5 g) was set prior to the displacement-driven testing protocol and, after preconditioning, a constant speed of 1 mm/min was applied to four electromagnetic motors for loading the specimen under equibiaxial condition. Two 200 N load cells were used to record forces along material directions. Data analysis to obtain stress and strain were calculated as defined in the constitutive modeling section.

2.3. Constitutive modeling

FEAs were carried out using two specific classes of materials: a) the isotropic Yeoh material model in the two-term formulation proposed by Raghavan and Vorp [9] for abdominal aortic aneurysms, and b) the orthotropic Fung-exponential model that is often used in soft tissue biomechanics. Both models adopt homogenous, incompressible and hyperplastic description of ATAA wall mechanics.

In short, the two-term Yeoh constitutive model relates the stress tenors (S) in the loaded specimen to the stretch (λ) through the equation:

$$S_{11} = S_{22} = [2\, c_1^{(Y)} + 4\, c_2^{(Y)}\, (\lambda^2 + 2\,\lambda^{-1} - 3)][\lambda^2 - \lambda^{-1}] \quad (1)$$

with $c_1^{(y)}$ and $c_2^{(y)}$ are material model parameters indicative of the mechanical properties of the ATAA wall, and λ is equal to the deformed specimen length divided by the original length. $S_{33} = 0$ according to the membrane stress state assumption adopted in our FEA approach.

The free energy function for the Fung model was:

$$\phi(\mathbf{C}) = \frac{c_1^{(F)}}{2}[\exp[Q(\mathbf{C})] - 1] \quad (2)$$

with $[c_1^{(F)}] = F/L$ the material-like parameter, $\mathbf{C} = \mathbf{F}^T\mathbf{F}$ the right Cauchy-Green strain tensor while the material-dependent exponent, $Q(\boldsymbol{C})$, was a quadratic form of Cauchy-Green strain tensor $\mathbf{C} = \mathbf{F}^T\mathbf{F}$:

$$Q(\mathbf{C}) = a_1\lambda_1^2 + a_2\lambda_2^2 + 2a_3\lambda_1\lambda_2 \quad (3)$$

with a_1, a_2, a_3 the dimensionless parameter.

The Cauchy stresses of Fung constitutive formulation are therefore expressed as:

$$\sigma_{11} = 2\lambda_1^2 c_1^{(F)} e^Q (a_1\lambda_1 + a_3\lambda_2)\sigma_{22} = 2\lambda_2^2 c_1^{(F)} e^Q (a_3\lambda_1 + a_2\lambda_2) \quad (4\text{ a,b})$$

2.4. Constitutive material parameter estimation

The elastostatic analysis for the evaluation of material constitutive parameters proposed by Liu et al. [23] is based on the main premise for which the stress distribution is statically determinate. Thus, for a given ATAA deformed configuration (ie, peak of systole) and known loading

condition (ie, the diastolic-to-systolic displacement field), different material parameters and constitutive models will give nearly the same stress field. In this way, an "almost-true" stress field at systole can be approximately obtained by an infinitesimal linear elastic model with sufficiently stiff material parameters. This fact has been theoretically justified by Miller and Lu [28] and numerically verified by Lu et al. [29] and Joldes et al. [22]. Given the constitutive model with an initial guess of material parameters (ie, $c_1^{(y)}$ and $c_2^{(y)}$for Yeoh model and $c_1^{(F)}$, a_1, a_2, a_3 for the Fung model), by using the constitutive equations and deformation relationship between the two loading states, an optimization algorithm allows to find the "true" material parameters such that the difference between the estimated and "almost-true" stress fields is minimized. Thus, the objective of the optimization process was to find a set of material descriptors that minimize the difference between the "almost-true" systolic stress, $\tilde{\sigma}^t$, and estimated systolic stress, $\tilde{\sigma}^{est}$, for each element as:

$$g_e^{(Y)} = \sum_{m=1}^{N}\sum_{i=1}^{2}[\tilde{S}_i^{(t)} - \tilde{S}_i^{(e)}(c_1^{(Y)}, c_2^{(Y)})]^2$$
$$g_e^{(F)} = \sum_{m=1}^{N}\sum_{i=1}^{2}[\tilde{S}_i^{(t)} - \tilde{S}_i^{(F)}(c_1^{(F)}, a_1, a_2, a_3)]^2 \quad (5\ a,b)$$

where N is the number of elements used in each model and i is the component index of each principal stress component. Eq. (1) and Eq. (4) were used for the estimated systolic stress of Yeoh and Fung models, respectively.

The optimization was implemented in the mathematical language program, MATLAB (v2018, Mathworks, MA, USA). Nonlinear least-squares algorithm with trust-region-reflective was used for the optimization of Yeoh material parameters using $c_1^{(Y)} > 0$ and $c_2^{(Y)} > 0$ as lower bounds. For the Fung-exponential form, physically meaningful and plausible material parameters were obtained by enforcing the convexity of the strain energy function and thus performing constrained minimization. For planar biaxial loading of soft tissue, strict convexity physically implies that the projections of the contour of $\phi(\mathbf{C})$on the $\lambda_1 - \lambda_2$plane form a convex surface [30]. It can be shown that if $c_1^{(F)} > 0$, then Eq. (4) is likely convex if and only if $a_1 > 0$, $a_2 > 0$ and. $a_1 a_2 - a_3^2 > 0$

For the estimation of the "almost-true" systolic stress distribution, we selected a very stiff material for the aortic wall (E = 2×10^4 GPa and v = 0.49) to obtain Cauchy stress. As initial guess of material descriptors, we used the population-average material properties reported by Pasta et al. [31] for the two-term Yeoh model and by Azdani et al. [32] for the Fung model of ATAAs. For each optimization procedure, principal stresses were imported in MATALB by postprocessing of ABAQUS models, and the optimization was done to obtain the optimal material parameters.

2.5. Computational study

ECG-gated CT images were used to segment the ATAA wall at both end-diastolic and peak-systolic cardiac phases using the medical imaging software Mimics (Mimics v20, Materialise, Leuven, BE) [15,33]. Semi-automatic threshold-based segmentation of aortic lumen allowed us to obtain a point cloud (resolution of 0.3 mm), which was triangulated to generate a surface mesh of both diastolic and systolic ATAA geometries. Using an algorithm previously developed by our group in MATLAB (v2018, Mathworks, MA, USA), the point cloud of the diastolic aortic-luminal surface was projected normally onto the systolic aortic-luminal surface to determine the displacement field as the Euclidean distance between closest points [15]. The estimated diastolic-to-systolic displacement field was then implemented as a boundary condition in the FEA model for estimating wall stresses.

For each patient, FEAs were developed using the reconstructed ATAA geometry at diastole, which was meshed with quadrilateral (M3D4R) and triangular (M3D3) membrane elements in ABAQUS/Explicit (v2018, SIMULIA Inc, Providence, RI). Reduced integration was used for the 4-node quadrilateral membrane element. Grid convergence led to an element size of 0.7 mm (element range of 28,200–37,500) to obtain a reproducible stress analysis of the human thoracic aorta [34]. Uniform material properties were adopted for the aortic wall while thickness measured from tissue samples was set for each patient simulation. Distal ends of the descending aorta and supra-aortic vessels were fixed in all directions. Material fiber direction was set using multiple cylindrical coordinate systems with origins in the centerline of the aneurysmal aorta. The ATAA wall was modeled using two constitute formulations to assess the role of the isotropic- and anisotropic material behavior on the resulting stress distribution. The density of the aortic tissue was 1060 kg/m^3. In the Abaqus/Explicit solver, ATAA wall mechanics was modeled as a quasi-static process while the energy was monitored to ensure the ratio of kinetic energy to internal energy remains less than 10%. Adequate time step was applied while an element-by-element stable time increment estimate, coupled with a "variable mass scaling technique," reduced the computational cost of each simulation. Mass scaling was performed by scaling the masses of elements whose stable time increments was less than the user-supplied time increment of 1.e−7 s so that the element stable time increment for these elements becomes equal to the user-supplied time increment. This approach has a minor effect on the stress analysis.

The numerical strategy is here summarized:

1. For the estimation of the "almost-true" stress distribution, the FEA model of each patient was loaded with a uniform peak systolic pressure distribution of 120 mmHg in a very stiff aortic wall (E = 2×10^4 GPa and v = 0.49). This approach led to infinitesimal deformation of aneurysmal aorta.
2. The resulting "almost-true" stress distribution was adopted to optimize the population-average material descriptors of Yeoh and Fung constitutive relationships. This step allowed us to find the optimal material parameters specific to a given patient geometry.
3. A second set of simulations was performed using the optimal material properties and the diastolic-to-systolic displacement field (instead of the uniform pressure distribution) to find realistic deformation of ATAA wall.
4. A third set of simulations was carried out using the displacement field as the boundary condition but using the experimental material properties evaluated from *ex-vivo* material testing. Then, results were compared to those observed for the second set of simulations.

3. Results

3.1. Experimental biaxial testing

Experimental raw data from equibiaxial testing are shown as Piola-Kirchhoff stress versus engineering-strain plots for ATAAs in both circumferential and longitudinal directions of ascending aorta (Fig. 1). Most of stress-strain data presented a linear part, related to the elastic properties of the aneurysmal aortic tissue, followed by an exponential part related to the collagen fiber recruitment. These parts were separated by the "yield point", which is more likely to define the *in-vivo* stress range. For a given tissue specimen, there was no remarkable difference of material response between longitudinal and circumferential directions, suggesting isotropic mechanical behavior for ATAA wall as previously found [31]. Stress-strain data were successfully fit by both the isotropic and anisotropic constitutive models, and the material parameters for each patient were estimated (Table 2). Fitting was able to accurately reproduce the non-linear behavior of experimental data ($R^2 > 0.91$ in all cases) so that material descriptors can be considered as determinants of the biomechanical behavior of ATAA wall. After running the elastostatic optimization analysis, material parameters were found close to those obtained from the fitting of the experimental stress-strain curves. We observed that even a variation of 10% on the

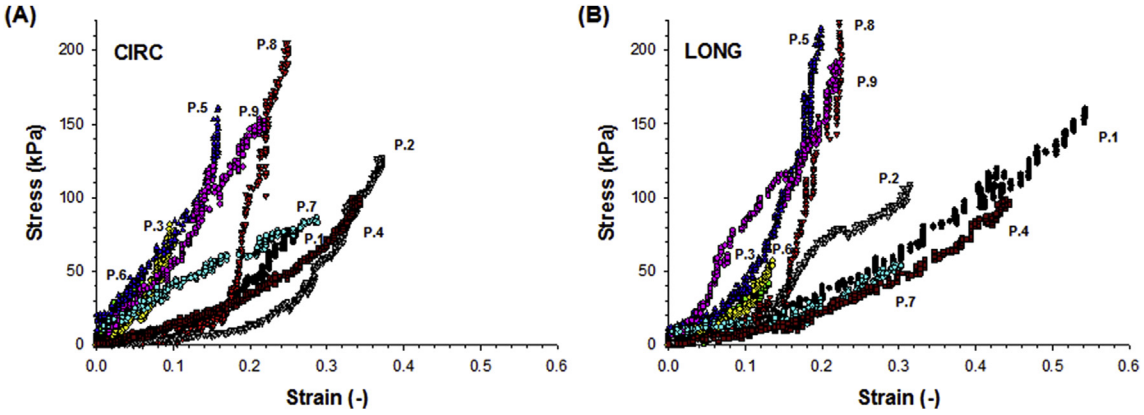

Fig. 1. Equibiaxial raw stress-strain data for ATAA specimens in (A) circumferential (CIRC) and (B) longitudinal (LONG) directions; labels indicate specimens obtained from same patient.

Table 2
Constitutive material parameters as obtained by the fitting of experimental biaxial testing (exp) and by the elastostatic optimization procedure (opt); coefficient of determination (R^2) refer to experimental data.

Patient ID	Yeoh				Fung				
		c_1^y (kPa)	c_2^y (kPa)	R^2	c_1^F	a_1	a_2	a_3	R^2
P.1	exp	13.1	147.9	0.990	5.6	6.7	6.6	4.7	0.970
	opt	21.6	157.5		27.1	13.8	8.7	5.5	
P.2	exp	31.1	42.6	0.990	29.9	32.3	53.2	12.4	0.984
	opt	38.6	43.1		112.1	8.9	8.2	7.5	
P.3	exp	64.9	134.5	0.980	42.0	15.4	1.0	1.4	0.990
	opt	84.2	35.4		110.0	4.4	15.2	8.2	
P.4	exp	38.4	101.1	0.990	55.8	3.1	10.6	0.1	0.991
	opt	27.0	169.7		6.6	1.2	2.4	0.5	
P.5	exp	75.6	884.0	0.970	14.5	29.2	31.1	1.7	0.982
	opt	50.1	560.0		4.5	12.02	13.1	12.6	
P.6	exp	50.4	75.1	0.998	32.8	8.1	12.7	1.2	0.978
	opt	96.4	42.1		96.8	14.3	12.4	4.8	
P.7	exp	3.8	86.7	0.990	99.7	2.5	3.8	−0.2	0.998
	opt	55.2	32.6		15.9	14.1	15.1	3.0	
P.8	exp	15.4	242.0	0.974	5.8	21.9	20.5	−7.8	0.935
	opt	51.2	480.9		42.1	26.3	26.2	−21.0	
P.9	exp	121.8	446.8	0.968	55.6	11.0	0	0.0	0.914
	opt	163.4	240.7		54.1	14.2	66.1	30.7	

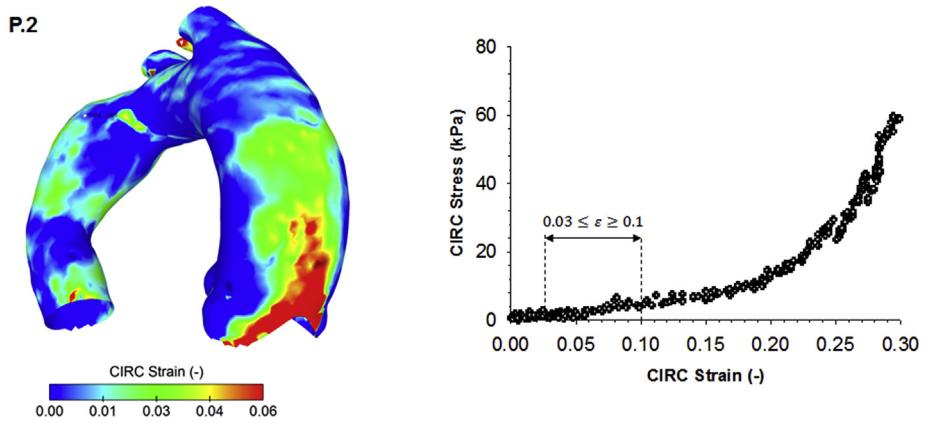

Fig. 2. Representative distribution of circumferential strain for patient P.2 as obtained after optimization procedure and raw stress-strain data in the circumferential direction showing the range of strain.

initial guess of the constitutive parameter set did not determine remarkable changes on the optimal material parameters.

3.2. Strain analysis

Fig. 2 shows the distribution of diastolic-to-systolic strain field as well as the experimental stress-strain curve from biaxial testing of the aortic tissue specimen cut from the same patient. It can be observed that the range of "true" strain in the circumferential direction is below the yield strain, which is the value of the strain at yield point before reaching the steep increase in the stress-strain response of tested aortic tissue specimen. Most of patients experienced low strain at CT imaging,

Table 3
Range of strain determined from CT imaging (ε_{CIRC}) and corresponding yield strain (ε_{yield}) extrapolated from stress-strain raw data of biaxial testing.

	P.1		P.2		P.3		P.4		P.5		P.6		P.7		**P.8**		P.9	
	min	max	min	max	min	max	min	max	min	max	min	max	min	max	**min**	max	min	max
ε_{CIRC}	0.01	0.15	0.01	0.03	0.04	0.15	0.03	0.12	0.02	0.18	0.01	0.16	0.01	0.13	0.05	0.10	0.01	0.13
ε_{yield}	0.16		0.24		0.25		0.17		0.15		0.09		0.21		0.17		0.08	

Fig. 3. Distribution of "almost-true" stress determined using a very stiff material for the aortic wall as compared to stress from the optimal material properties for the Yeoh and Fung constitutive models of P.1.

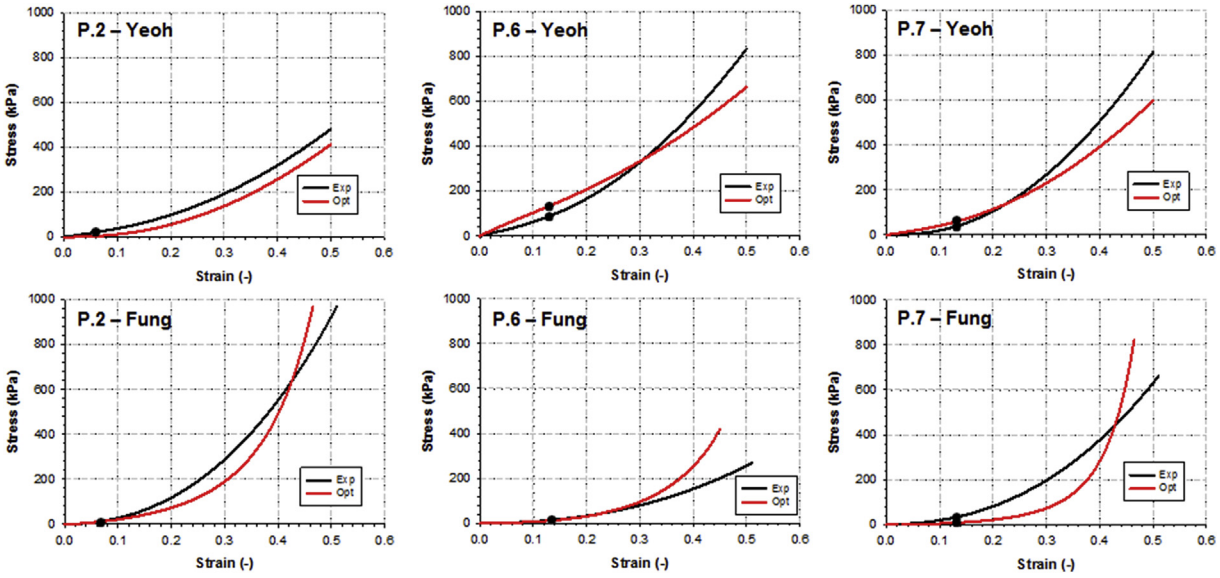

Fig. 4. Comparison of stress-strain response curves under equibiaxial loading condition for three representative patients as modeled with two-term Yeoh constitutive model (top row) and Fung-exponential model (bottom row) using experimental and optimized material parameters; dots indicates maximum value of peak systolic strain.

except for patients P.6 and P.9 who experience strains remarkably above the yield strain (Table 3). This can be determined by high blood pressure induced by hypertension, increased stretch and twist of aortic vessel due to heart beating and local changes of material properties or tissue thickness, exposing the aneurysmal aorta at greater risk of complications than other patients.

3.3. "Almost-true" stress computation

The distribution of "almost-true" stress determined by the simple linear-elastic FEA with the stiff elastic modulus was compared to that obtained at the end of optimization procedure for each patient simulation. Specifically, the maximum principal stress exerted on the ATAA wall was used as an indicator of intramural stress of aneurysmal aorta. Fig. 3 shows that the stiff ATAA model had a stress distribution similar to that of Fung model but different from that shown by the Yeoh model. The mean absolute percentage error (MAPE) was calculated for each patient as a measure of differences among simulation approaches. For the patient P.1 shown in Fig. 3, the MAPE was nearly 30% between the "almost-true" and Yeoh models and 8.5% between the "almost-true" and Fung models. For other patient cases, we found errors in the range of 6–18%.

3.4. Biaxial testing of optimal vs experimental material parameters

Optimized material parameters obtained from elastostatic analysis were used to determine the stress-strain response under equibiaxial loading conditions in a FEA reproducing the experimental testing of

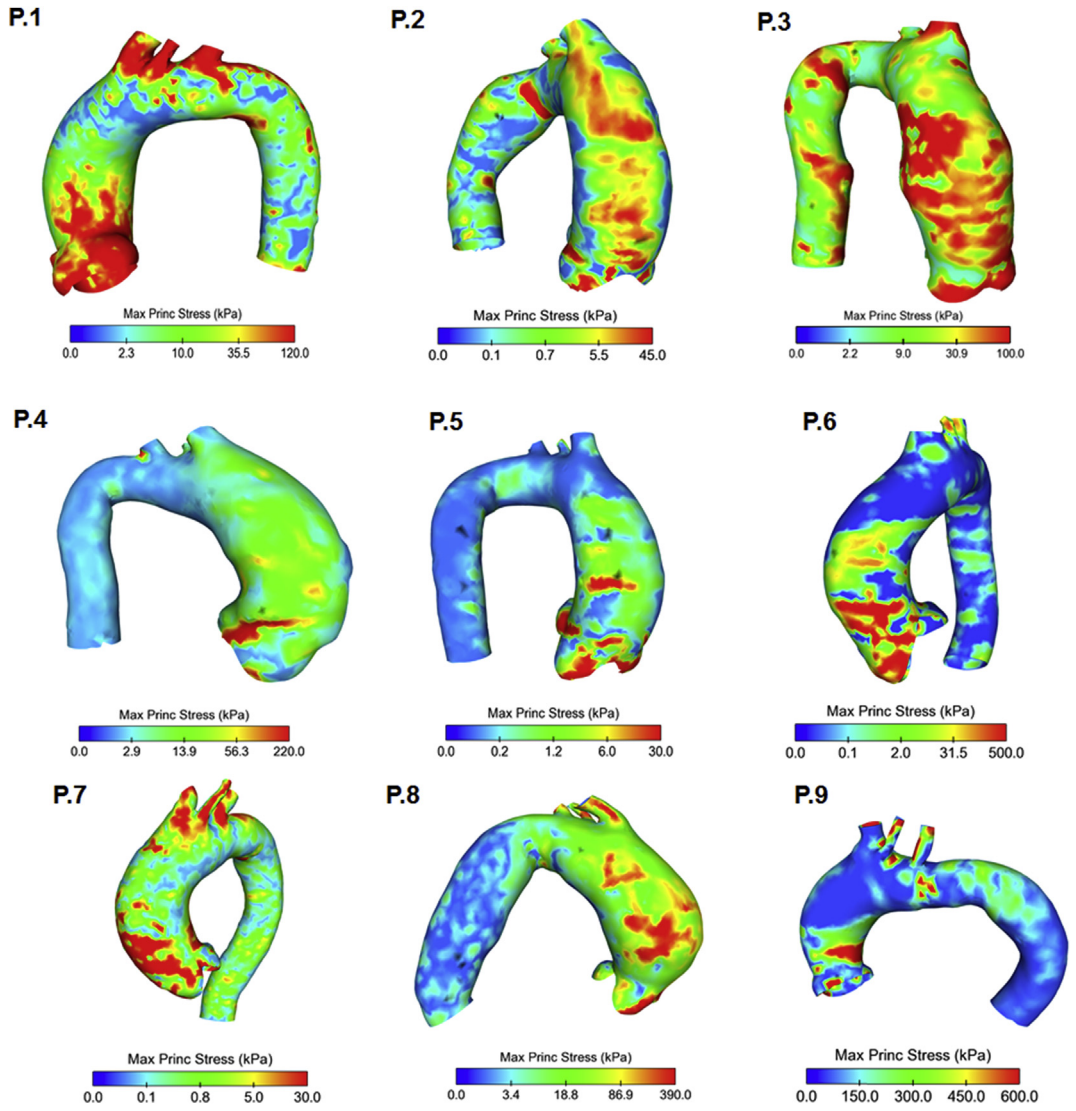

Fig. 5. Distribution of patients-specific stress as quantified by the maximum principal stress at peak systole for all patients using the Yeoh constitutive material formulation based on the fitting of experimental data.

aortic tissue sample. Then, the stress-strain curves were plotted together with the experimental testing data (see Fig. 4). P.2 with small strain field exhibited a practically equivalent stress-strain response with both experimental and elastostatic material descriptors. At strain of 14%, P.6 had the largest discrepancy of 24% in stress predictions between optimized and experimental material descriptors of two-term Yeoh constitutive model.

3.5. Patient-specific FEA of optimal vs experimental material parameters

Fig. 5 illustrates predicted wall stress distributions computed by patient-specific material descriptors determined from experimental biaxial testing of Yeoh model. Local maxima of wall stress were mainly placed near the maximum curvature of the ascending aorta, just above the sino-tubular junction. In a similar way, Fig. 6 shows predicted wall stress maps resulting from the experimentally-based material fitting using the Fung model. It can be observed that stress distributions are similar among constitutive formulations (ie, Yeoh versus Fung model) when patient-specific material parameters are adopted.

Although biaxial testing results of optimal versus experimental material parameters are encouraging, we found considerable discrepancies for the patient-specific stress predictions between the optimal material parameter set versus the experimentally-derived set (Fig. 7). The MAPE was calculated for each patient and evinced highly variable differences from patient to patient and the type of constitutive formulation (see Table 4).

4. Discussion

In this study, we exploited the appealing concept of obtaining reasonably and accurate stress solutions of aneurysm mechanics using an inverse approach, and thus without invoking accurate material descriptors that are hard to know before surgical management of ATAAs. We optimized population-average material parameters with respect to a “the “almost-true” stress fields obtained with an infinitesimal linear-elastic model based on a sufficiently stiff Young modulus [23]. The so-recovered material parameters were implemented in FEAs, and then stress distributions of nine ATAA geometries were compared to those predicted when patient-specific material descriptors are estimated from the fitting of *ex-vivo* testing data of aortic tissue specimens collected from the same patient. We observed that the stress-strain response under equibiaxial loading predicted by the elastostatic analysis was consistent to the experimental material behavior if strain was low (largest difference of 24% at strain of 14%). This was in agreement with

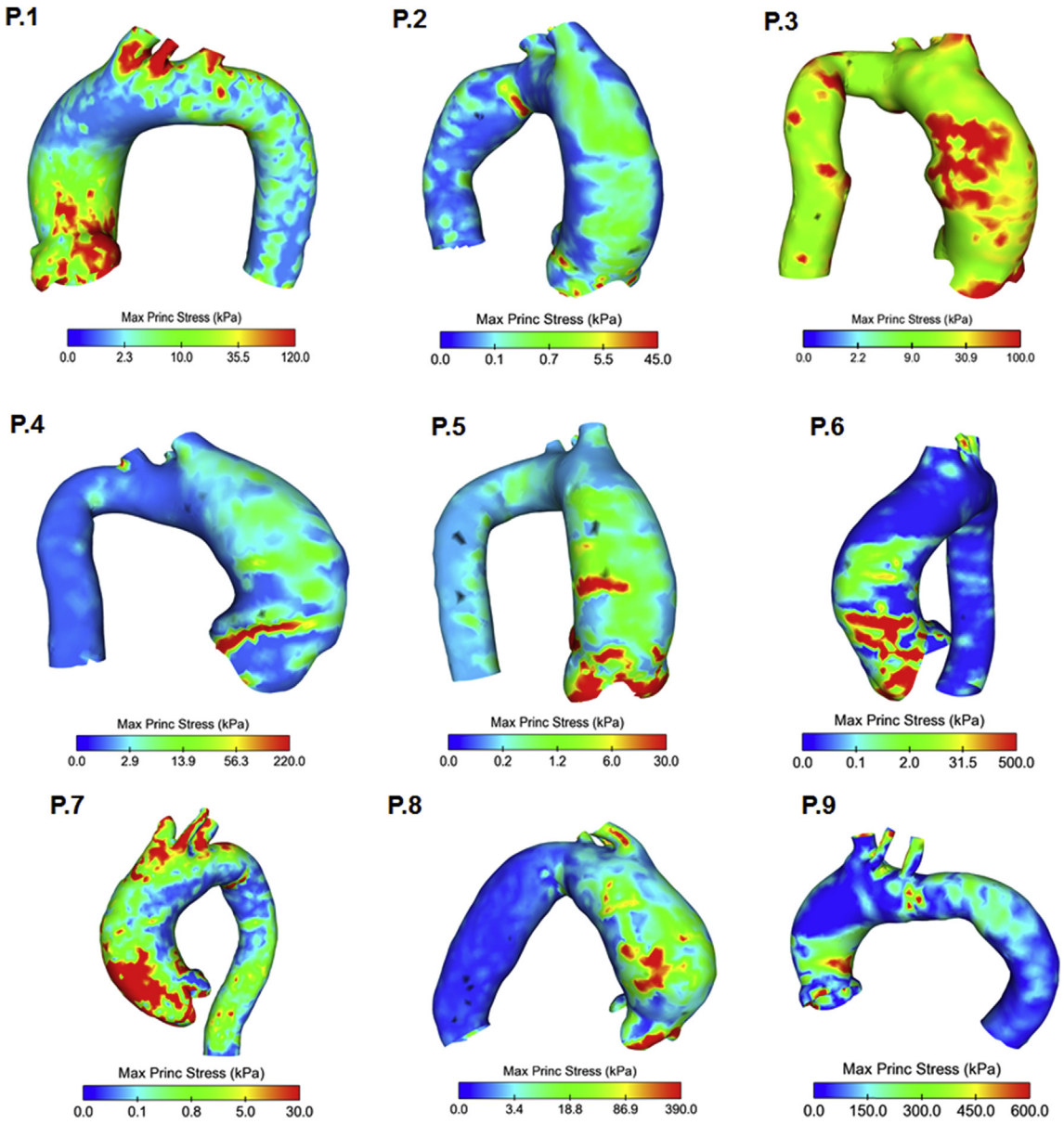

Fig. 6. Distribution of patients-specific stress as quantified by the maximum principal stress at peak systole for all patients using the Fung constitutive material formulation based on the fitting of experimental data.

findings documented by Liu et al. [23]. However, the discrepancy on predicted stress distributions was considerably, depending on the adopted constitutive model and ATAA shape, when FEAs were performed on patient anatomies. Although the stress analysis of abdominal aortic aneurysms did not depend on material properties [22], the modeling of the ascending aorta as a statically-determinate structure needs further understanding so that the role of material properties is still important for realistic and accurate stress predictions.

Identification of patient-specific material parameters of ATAAs deserves important interest as FEAs rely on population-average values of material properties for those patients undergoing close monitoring of the aneurysm size. In risk predictions of aneurysm failure, FEAs based on patient-specific material descriptors were carried out in very few studies restricted to patients who underwent elective surgical repair of ATAA wall to derive the material behavior from uniaxial or bulge inflation tests [11,12]. The role of material properties in computational growth and remodeling analyses may be even more remarkable as stress estimations are strongly dependents on local material changes [35].

To avoid *ex-vivo* material testing, inverse approaches allows to estimate material descriptors; however, inverse analysis involves a complex non-linear problem [36,37]. Most of inverse techniques proposed for soft tissue mechanics attempt to minimize a cost function defined by the difference between a target parameter, which is determined from medical image analysis, and a candidate parameter estimated from FEA and then iteratively adjusted to tune material parameters of interest [38]. However, inverse approaches are commonly time consuming due to continuous interaction with the FEA solver [39]. For the ascending aorta, Trabelsi et al. [38] proposed an inverse method in which the target variable was the volume variation of the aorta measured from ECG-gated CT scans. They assumed a linear relationship between the constitutive material parameter and the volume of the aortic luminal surface, and then carried out eight FEA analyses for each patient to build datasets for several CT measurements of ATAA volume at systole and mid-cardiac phase. The error attributed to this approach was 0.6% on estimated CT volume and 9.6% on the predicted stress response under equibiaxial test simulations. In agreement with our findings, the statically determinate inverse approach proposed by Liu et al. [23] for the Gasser-Holzapfel-Ogden constitutive model

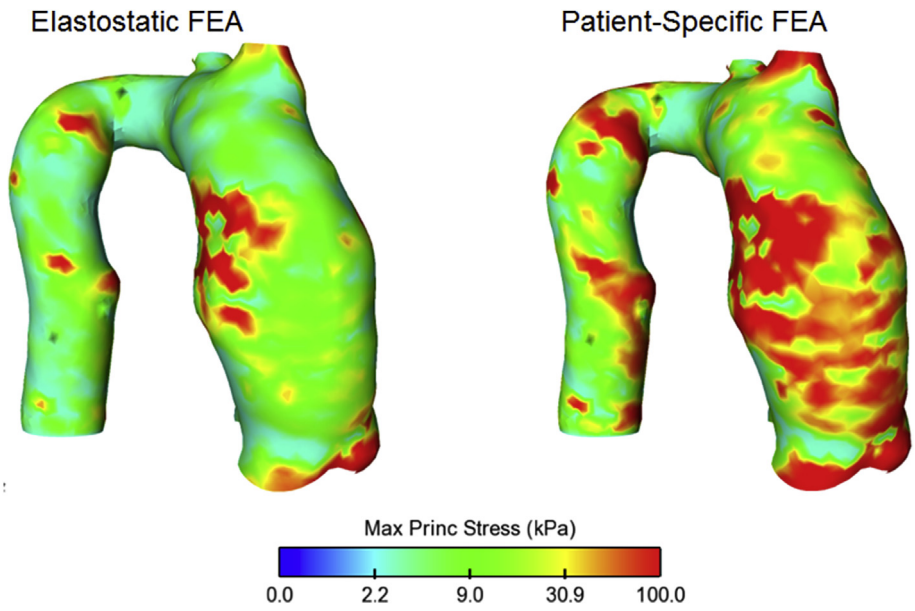

Fig. 7. Comparisons of stress distribution for P.3 using the material parameters obtained by the FEA using the statically-determinate optimization procedure versus the FEA using patient-specific material parameters.

Table 4
Mean absolute percentage error (MAPE) of maximum principal stress between experimentally-derived and optimized material parameters.

	P.1	P.2	P.3	P.4	P.5	P.6	P.7	P.8	P.9
Yeoh	0.7105	0.7398	0.7545	0.4520	0.5303	0.7034	0.2138	0.1754	0.3245
Fung	0.7683	0.1140	0.6022	0.3241	0.7539	0.7130	0.0349	0.2198	0.7034

demonstrated comparable biaxial stress-strain curves between elastostatic analyses and experimental tests estimated in a previous investigation of the same group [11]. In their patient study group, patient-specific FEAs on ATAA anatomies were not done because of lack of both CT and tissue data, without quantification of stress changes computed with either experimental or elastostatic-based material parameters.

Generally, the stress of a deformable body depends not only on its geometry, load and boundary conditions, but also on the mechanical properties of constituents. One of the obstacles standing before the biomechanics community is the difficulty in obtaining patient-specific properties of tissues given the absence of a methodology to non-invasively estimate stress *in-vivo*. Notwithstanding, there is an emerging interest from several groups in reformulating computational mechanics in a new paradigm so that computational stress predictions are weakly sensitive to the variation of mechanical properties when the deformed configuration is given [28]. This paradigm can apply to non-linear elastic material, because the stress in such material depends on the relative deformation among two definite configurations. If one of them is known, the other can be solved from equilibrium, which is dominated by in-plane stress for thin-walled structure treated as a membrane. From the analysis of ECG-gated CT images, we observed that strain at deformed configuration bears to the linear-elastic part of the experimental stress-strain response (see Table 3), thereby supporting in part the static determinacy of the aneurysmal wall. In this way, the inverse problem can be directly formulated using the constitutive law as here presented or shown by other studies [23,40] and without the need of a continuous interaction with the FEA solver. Using the Fung model, Miller et al. [28] investigated the sensitivity of the stress solution with respect to material parameters and constitutive model in three intracranial aneurysm geometries under static determinacy. The inverse stress solution was far less sensitive to material description as, for instance, the 100 times increase in the stiffness parameter C of the Fung model led to a 2.9% error in the maximum principal stress prediction. As compared to abdominal or cerebral aneurysms, the ascending aorta is cyclically stretched and twisted every heartbeat by determining the presence of longitudinal and shear stresses in a way that the static equilibrium is not only governed by the internal pressure. These mechanical forces are also highly dynamic (as systole is approximately 0.33s), thereby determining viscoelastic effects. These factors combined to residual stress likely occurring in blood vessels can pose several doubts on the modeling of the ascending aorta as statically-determinate structure.

The major limitation of this study is that comparisons of stress predictions were carried out assuming the experimentally-derived material parameters as the true material descriptors of the ATAA wall, but these can be indeed different from the *in-vivo* condition. However, there is no methodology to *in-vivo* estimate the material behavior so that experimental material parameters are the most accurate ATAA material descriptors. FEAs were based on homogenous thickness and material properties for the whole aorta but there exist evidence of regional changes in the material properties and thickness along the vessel circumference [41] and from the aortic root to the distal ascending aorta [42]. It should be mentioned that the optimization procedure can be modified to account for heterogenous thickness and regionally-dependent material properties by slightly altering the workflow and evaluating the objective function element-by-element. Disregarding the presence of residual stresses and considering the arterial wall as a 3D membrane with uniform thickness can be considered as additional limitations of the current work. It was assumed that the aortic wall behaves as a membrane with no bending moments or no through thickness shear, although regions near the branches may not satisfy the membrane assumption. The orientation of elastic fiber was not considered in FEAs, and this may alter the stress distribution as demonstrated in a previous study [31]. Caliper-based measurements of tissue thickness can lead to errors which in turn affect aortic wall stress

predictions.

5. Conclusion

We conclude that the modeling of the ascending aorta as a statically determinate can lead to errors on wall stress predictions in patient-specific FEAs since aortic wall stress was found to depend on the type of constitutive model and ATAA geometry. Static determinacy needs better understanding of its application to determine ascending aortic aneurysm mechanics so that patient-specific material descriptors as determined by *ex-vivo* material testing are advocated for reliable accurate stress predictions of ATAA wall mechanics.

Conflicts of interest

None.

Acknowledgments

This work was supported by a “Ricerca Finalizzata” grant from the Italian Ministry of Health (GR-2011-02348129) as well as by a grant from Fondazione RiMED to Salvatore Pasta. Federica Cosentino thanks the Fondazione RiMED and Ministry of Education, University and Research (MIUR) for supporting her PhD programme.

References

[1] L.K. Bickerstaff, P.C. Pairolero, L.H. Hollier, L.J. Melton, H.J. Van Peenen, K.J. Cherry, J.W. Joyce, J.T. Lie, Thoracic aortic aneurysms: a population-based study, Surgery 92 (1982) 1103–1108.

[2] M.A. Coady, J.A. Rizzo, G.L. Hammond, D. Mandapati, U. Darr, G.S. Kopf, J.A. Elefteriades, O.W. Isom, F. Robicsek, R.B. Griepp, What is the appropriate size criterion for resection of thoracic aortic aneurysms? J. Thorac. Cardiovasc. Surg. 113 (1997) 476–491.

[3] J.A. Beckman, Aortic aneurysms: pathophysiology, epidemiology and prognosis, in: M.A. Creager, V.J. Dzau, J. Loscalzo (Eds.), Vascular Medicine, Saunders Elsevier, Philadelphia, PA, 2006.

[4] S. Verma, S.C. Siu, Aortic dilatation in patients with bicuspid aortic valve, N. Engl. J. Med. 370 (2014) 1920–1929.

[5] M.A. Borger, P.W.M. Fedak, E.H. Stephens, T.G. Gleason, E. Girdauskas, J.S. Ikonomidis, A. Khoynezhad, S.C. Siu, S. Verma, M.D. Hope, D.E. Cameron, D.F. Hammer, J.S. Coselli, M.R. Moon, T.M. Sundt, A.J. Barker, M. Markl, A. Della Corte, H.I. Michelena, J.A. Elefteriades, The American Association for Thoracic Surgery consensus guidelines on bicuspid aortic valve-related aortopathy: Full online-only version, J. Thorac. Cardiovasc. Surg. 156 (2018) e41–e74.

[6] A. Della Corte, C. Bancone, C. Quarto, G. Dialetto, F.E. Covino, M. Scardone, G. Caianiello, M. Cotrufo, Predictors of ascending aortic dilatation with bicuspid aortic valve: a wide spectrum of disease expression, Eur. J. Cardiothorac. Surg. 31 (2007) 397–404 discussion 404-395.

[7] J.A. Elefteriades, E.A. Farkas, Thoracic aortic aneurysm clinically pertinent controversies and uncertainties, J. Am. Coll. Cardiol. 55 (2010) 841–857.

[8] L.A. Pape, T.T. Tsai, E.M. Isselbacher, J.K. Oh, P.T. O'Gara, A. Evangelista, R. Fattori, G. Meinhardt, S. Trimarchi, E. Bossone, T. Suzuki, J.V. Cooper, J.B. Froehlich, C.A. Nienaber, K.A. Eagle, Aortic diameter > = 5.5 cm is not a good predictor of type A aortic dissection - observations from the international registry of acute aortic dissection (IRAD), Circulation 116 (2007) 1120–1127.

[9] M.L. Raghavan, D.A. Vorp, Toward a biomechanical tool to evaluate rupture potential of abdominal aortic aneurysm: identification of a finite strain constitutive model and evaluation of its applicability, J. Biomech. 33 (2000) 475–482.

[10] M.F. Fillinger, S.P. Marra, M.L. Raghavan, F.E. Kennedy, Prediction of rupture risk in abdominal aortic aneurysm during observation: wall stress versus diameter, J. Vasc. Surg. 37 (2003) 724–732.

[11] C. Martin, W. Sun, T. Pham, J. Elefteriades, Predictive biomechanical analysis of ascending aortic aneurysm rupture potential, Acta Biomater. 9 (2013) 9392–9400.

[12] O. Trabelsi, F.M. Davis, J.F. Rodriguez-Matas, A. Duprey, S. Avril, Patient specific stress and rupture analysis of ascending thoracic aneurysms, J. Biomech. 48 (2015) 1836–1843.

[13] A.K. Venkatasubramaniam, M.J. Fagan, T. Mehta, K.J. Mylankal, B. Ray, G. Kuhan, I.C. Chetter, P.T. McCollum, A comparative study of aortic wall stress using finite element analysis for ruptured and non-ruptured abdominal aortic aneurysms, Eur. J. Vasc. Endovasc. Surg. 28 (2004) 168–176.

[14] L. Liang, M. Liu, C. Martin, J.A. Elefteriades, W. Sun, A machine learning approach to investigate the relationship between shape features and numerically predicted risk of ascending aortic aneurysm, Biomechanics Model. Mechanobiol. 16 (2017) 1519–1533.

[15] S. Pasta, G. Gentile, G.M. Raffa, D. Bellavia, G. Chiarello, R. Liotta, A. Luca, C. Scardulla, M. Pilato, In silico shear and intramural stresses are linked to aortic valve morphology in dilated ascending aorta, european journal of vascular and endovascular surgery, the official journal of the European Society for Vascular Surgery 54 (2017) 254–263.

[16] A. Rinaudo, S. Pasta, Regional variation of wall shear stress in ascending thoracic aortic aneurysms, Proc. IME H J. Eng. Med. 228 (2014) 627–638.

[17] J.J. Lee, G. D'Ancona, A. Amaducci, F. Follis, M. Pilato, S. Pasta, Role of computational modeling in thoracic aortic pathology: a review, J. Card. Surg. 29 (2014) 653–662.

[18] G. D'Ancona, A. Amaducci, A. Rinaudo, S. Pasta, F. Follis, M. Pilato, R. Baglini, Haemodynamic predictors of a penetrating atherosclerotic ulcer rupture using fluid-structure interaction analysis, Interact. Cardiovasc. Thorac. Surg. 17 (2013) 576–578.

[19] A.J. Barker, C. Lanning, R. Shandas, Quantification of hemodynamic wall shear stress in patients with bicuspid aortic valve using phase-contrast MRI, Ann. Biomed. Eng. 38 (2010) 788–800.

[20] S. Pasta, V. Agnese, M. Di Giuseppe, G. Gentile, G.M. Raffa, D. Bellavia, M. Pilato, In vivo strain analysis of dilated ascending thoracic aorta by ECG-gated CT angiographic imaging, Ann. Biomed. Eng. 45 (2017) 2911–2920.

[21] H. Haraldsson, M. Hope, G. Acevedo-Bolton, E. Tseng, X. Zhong, F.H. Epstein, L. Ge, D. Saloner, Feasibility of asymmetric stretch assessment in the ascending aortic wall with DENSE cardiovascular magnetic resonance, J. Cardiovasc. Magn. Reson. 16 (2014) 6.

[22] G.R. Joldes, K. Miller, A. Wittek, B. Doyle, A simple, effective and clinically applicable method to compute abdominal aortic aneurysm wall stress, J. Mech. Behav. Biomed. Mater. 58 (2016) 139–148.

[23] M. Liu, L. Liang, W. Sun, A new inverse method for estimation of in vivo mechanical properties of the aortic wall, J. Mech. Behav. Biomed. Mater. 72 (2017) 148–158.

[24] S. Farzaneh, O. Trabelsi, S. Avril, Inverse Identification of Local Stiffness across Ascending Thoracic Aortic Aneurysms, Biomech Model Mechanobiol, 2018.

[25] L. Liang, M. Liu, C. Martin, W. Sun, A deep learning approach to estimate stress distribution: a fast and accurate surrogate of finite-element analysis, J. R. Soc. Interface 15 (2018).

[26] B.J. Doyle, P.E. Norman, P.R. Hoskins, D.E. Newby, M.R. Dweck, Wall stress and geometry of the thoracic aorta in patients with aortic valve disease, Ann. Thorac. Surg. 105 (2018) 1077–1085.

[27] V. Mendez, M. Di Giuseppe, S. Pasta, Comparison of hemodynamic and structural indices of ascending thoracic aortic aneurysm as predicted by 2-way FSI, CFD rigid wall simulation and patient-specific displacement-based FEA, Comput. Biol. Med. 100 (2018) 221–229.

[28] K. Miller, J. Lu, On the prospect of patient-specific biomechanics without patient-specific properties of tissues, J. Mech. Behav. Biomed. Mater. 27 (2013) 154–166.

[29] J. Lu, X.L. Zhou, M.L. Raghavan, Inverse method of stress analysis for cerebral aneurysms, Biomechanics Model. Mechanobiol. 7 (2008) 477–486.

[30] G.A. Holzapfel, T.C. Gasser, R.W. Ogden, A new constitutive framework for arterial wall mechanics and a comparative study of material models, J. Elast. 61 (2000) 1–48.

[31] S. Pasta, J.A. Phillippi, A. Tsamis, A. D'Amore, G.M. Raffa, M. Pilato, C. Scardulla, S.C. Watkins, W.R. Wagner, T.G. Gleason, D.A. Vorp, Constitutive modeling of ascending thoracic aortic aneurysms using microstructural parameters, Med. Eng. Phys. 38 (2016) 121–130.

[32] A.N. Azadani, S. Chitsaz, A. Mannion, A. Mookhoek, A. Wisneski, J.M. Guccione, M.D. Hope, L. Ge, E.E. Tseng, Biomechanical properties of human ascending thoracic aortic aneurysms, Ann. Thorac. Surg. 96 (2013) 50–58.

[33] S. Pasta, A. Rinaudo, A. Luca, M. Pilato, C. Scardulla, T.G. Gleason, D.A. Vorp, Difference in hemodynamic and wall stress of ascending thoracic aortic aneurysms with bicuspid and tricuspid aortic valve, J. Biomech. 46 (2013) 1729–1738.

[34] D.P. Nathan, C. Xu, J.H. Gorman III, R.M. Fairman, J.E. Bavaria, R.C. Gorman, K.B. Chandran, B.M. Jackson, Pathogenesis of acute aortic dissection: a finite element stress analysis, Ann. Thorac. Surg. 91 (2011) 458–463.

[35] G. Martufi, T.C. Gasser, J.J. Appoo, E.S. Di Martino, Mechano-biology in the thoracic aortic aneurysm: a review and case study, Biomechanics Model. Mechanobiol. 13 (2014) 917–928.

[36] J.E. Zelaya, S. Goenezen, P.T. Dargon, A.F. Azarbal, S. Rugonyi, Improving the efficiency of abdominal aortic aneurysm wall stress computations, PLoS One 9 (2014) e101353.

[37] J. Biehler, M.W. Gee, W.A. Wall, Towards efficient uncertainty quantification in complex and large-scale biomechanical problems based on a Bayesian multi-fidelity scheme, Biomechanics Model. Mechanobiol. 14 (2015) 489–513.

[38] O. Trabelsi, A. Duprey, J.P. Favre, S. Avril, Predictive models with patient specific material properties for the biomechanical behavior of ascending thoracic aneurysms, Ann. Biomed. Eng. 44 (2016) 84–98.

[39] A. Wittek, K. Karatolios, C.P. Fritzen, J. Bereiter-Hahn, B. Schieffer, R. Moosdorf, S. Vogt, C. Blase, Cyclic three-dimensional wall motion of the human ascending and abdominal aorta characterized by time-resolved three-dimensional ultrasound speckle tracking, Biomechanics Model. Mechanobiol. 15 (2016) 1375–1388.

[40] M. Peirlinck, M. De Beule, P. Segers, N. Rebelo, A modular inverse elastostatics approach to resolve the pressure-induced stress state for in vivo imaging based cardiovascular modeling, J. Mech. Behav. Biomed. Mater. 85 (2018) 124–133.

[41] D.C. Iliopoulos, R.P. Deveja, E.P. Kritharis, D. Perrea, G.D. Sionis, K. Toutouzas, C. Stefanadis, D.P. Sokolis, Regional and directional variations in the mechanical properties of ascending thoracic aortic aneurysms, Med. Eng. Phys. 31 (2009) 1–9.

[42] A.N. Azadani, S. Chitsaz, P.B. Matthews, N. Jaussaud, J. Leung, T. Tsinman, L. Ge, E.E. Tseng, Comparison of mechanical properties of human ascending aorta and aortic sinuses, Ann. Thorac. Surg. 93 (2012) 87–94.